

Characterization of the four new transiting planets KOI-188b, KOI-195b, KOI-192b, and KOI-830b

G. Hébrard^{1,2}, A. Santerne^{3,4,5}, G. Montagnier^{1,2}, G. Bruno³, M. Deleuil³, M. Havel⁴, J.-M. Almenara³, C. Damiani³,
S. C. C. Barros³, A. S. Bonomo⁶, F. Bouchy³, R. F. Díaz^{3,7}, and C. Moutou³

¹ Institut d'astrophysique de Paris, UMR7095 CNRS, Université Pierre & Marie Curie, 98bis boulevard Arago, 75014 Paris, France
e-mail: hebrard@iap.fr

² Observatoire de Haute-Provence, CNRS/OAMP, 04870 Saint-Michel-l'Observatoire, France

³ Aix Marseille Université, CNRS, LAM (Laboratoire d'Astrophysique de Marseille) UMR 7326, 13388 Marseille, France

⁴ Centro de Astrofísica, Universidade do Porto, Rua das Estrelas, 4150-762 Porto, Portugal

⁵ Instituto de Astrofísica e Ciências do Espaço, Universidade do Porto, CAUP, Rua das Estrelas, 4150-762 Porto, Portugal

⁶ INAF - Osservatorio Astrofisico di Torino, Via Osservatorio 20, 10025 Pino Torinese, Italy

⁷ Observatoire astronomique de l'Université de Genève, 51 chemin des Maillettes, 1290 Versoix, Switzerland

Received TBC; accepted TBC

ABSTRACT

The characterization of four new transiting extrasolar planets is presented here. KOI-188b and KOI-195b are bloated hot Saturns, with orbital periods of 3.8 and 3.2 days, and masses of 0.25 and 0.34 M_{Jup} . They are located in the low-mass range of known transiting, giant planets. KOI-192b has a similar mass (0.29 M_{Jup}) but a longer orbital period of 10.3 days. This places it in a domain where only a few planets are known. KOI-830b, finally, with a mass of 1.27 M_{Jup} and a period of 3.5 days, is a typical hot Jupiter. The four planets have radii of 0.98, 1.09, 1.2, and 1.08 R_{Jup} , respectively. We detected no significant eccentricity in any of the systems, while the accuracy of our data does not rule out possible moderate eccentricities. The four objects were first identified by the *Kepler* Team as promising candidates from the photometry of the *Kepler* satellite. We establish here their planetary nature thanks to the radial velocity follow-up we secured with the HARPS-N spectrograph at the *Telescopio Nazionale Galileo*. The combined analyses of the datasets allow us to fully characterize the four planetary systems. These new objects increase the number of well-characterized exoplanets for statistics, and provide new targets for individual follow-up studies. The pre-screening we performed with the SOPHIE spectrograph at the *Observatoire de Haute-Provence* as part of that study also allowed us to conclude that a fifth candidate, KOI-219.01, is not a planet but is instead a false positive*.

Key words. Planetary systems – Techniques: radial velocities – Techniques: photometric – Techniques: spectroscopic – Stars: individual: KOI-188 (Kepler-425), KOI-192 (Kepler-427), KOI-195 (Kepler-426), KOI-219, KOI-830 (Kepler-428).

1. Introduction

Today, more than 3800 transiting planetary candidates have been identified from the data of the *Kepler* satellite. They have been obtained from the analyses of the light curves of the 156 000 stars with magnitudes $9 < V < 16$ continuously observed by *Kepler* from May 2009 to May 2013 with a high photometric accuracy. These candidates are designated as KOIs (Kepler Objects of Interest) in the successive announcements by the *Kepler* Team (e.g., Borucki et al. 2011a, 2011b; Batalha et al. 2013; Burke et al. 2013). Whereas several stellar configurations can mimic planetary transits (e.g., Almenara et al. 2009), it has been argued that contrary to ground-based or *CoRoT* photometric surveys, such false positives are rare among *Kepler* candidates and most of them should actually be planets (e.g., Morton & Johnson 2011). This is particularly the case for multiple-planet candidates (e.g., Lissauer et al. 2012, 2014). On the other hand, the proportion of false positives is expected to be significant among single, close-in, giant exoplanet KOI candidates, with a false positive rate of $34.8 \pm 6.5\%$ measured by Santerne et al. (2012), whereas Fressin

et al. (2013) predicted it to be $29.3 \pm 3.1\%$ from statistical arguments (both false positive rates are computed for periods shorter than 25 days). Such false positive rates are lower than those of ground-based and *CoRoT* photometric surveys but they remain significant. Some individual cases of KOI false positives have been presented, e.g., by Bouchy et al. (2011), Colòn et al. (2012), Díaz et al. (2013), or Moutou et al. (2013).

Follow-up analyses and/or observations are thus mandatory in order to identify which KOIs are actually planets, and which are not. Such identifications are essential in order to construct a sample of exoplanets free of false positives for unbiased statistical studies. This is also important for individual analyses of particular objects, as transiting planets allow numerous studies including atmospheric absorber detections or obliquity measurements. Radial velocity is a particularly rich follow-up observation method as it allows numerous stellar scenarios to be distinguished from actual planets among photometric candidates. For the identified planets, it also allows their masses and the eccentricity of their orbits to be measured. The planetary radii and masses are provided by transit light curves and radial velocities, respectively; the joint use of the two methods gives access to the planetary densities and deep characterizations.

Since 2010 we have been conducting radial-velocity follow-up of KOIs with the SOPHIE spectrograph at the *Observatoire*

* Table 6 is available only in electronic form at the CDS via anonymous ftp to cdsarc.u-strasbg.fr (130.79.128.5) or via <http://cdsweb.u-strasbg.fr/cgi-bin/qcat?J/A+A/>. CDS also includes the radial velocities given in Tables 2 and 3.

Table 1. IDs, coordinates, and magnitudes of the planet-host stars.

<i>Kepler</i> Object of Interest	KOI-188	KOI-195	KOI-192	KOI-830
<i>Kepler</i> exoplanet catalog	Kepler-425	Kepler-426	Kepler-427	Kepler-428
<i>Kepler</i> Input Catalog	KIC5357901	KIC11502867	KIC7950644	KIC5358624
USNO-A2 ID	1275-11218459	1350-10395462	1275-10946568	1275-11249110
2MASS ID	19212592+4034038	19174431+4928242	19130109+4342175	19221961+4034386
RA (J2000)	19:21:25.92	19:17:44.31	19:13:01.10	19:22:19.62
DEC (J2000)	+40:34:03.86	+49:28:24.24	+43:42:17.53	+40:34:38.64
<i>Kepler</i> magnitude K_p	14.74	14.84	14.22	15.22
Johnson- <i>V</i>	14.97 ± 0.04	15.073 ± 0.013	14.42 ± 0.02	15.405 ± 0.016
Johnson- <i>B</i>	16.047 ± 0.016	15.736 ± 0.021	15.13 ± 0.03	16.584 ± 0.046
SDSS- <i>G</i>	15.465 ± 0.014	15.293 ± 0.019	14.65 ± 0.03	15.931 ± 0.024
SDSS- <i>R</i>	14.73 ± 0.07	14.863 ± 0.035	14.31 ± 0.07	15.101 ± 0.037
SDSS- <i>I</i>	14.605 ± 0.22	14.735 ± 0.029	14.013 ± 0.019	14.84 ± 0.07
2MASS- <i>J</i>	13.376 ± 0.021	13.624 ± 0.026	13.161 ± 0.023	13.767 ± 0.024
2MASS- <i>H</i>	12.931 ± 0.020	13.230 ± 0.033	12.814 ± 0.022	13.295 ± 0.023
2MASS- <i>K_s</i>	12.806 ± 0.027	13.212 ± 0.033	12.777 ± 0.024	13.234 ± 0.033
WISE- <i>W1</i>	12.791 ± 0.025	13.200 ± 0.024	12.731 ± 0.023	13.142 ± 0.025
WISE- <i>W2</i>	12.864 ± 0.027	13.252 ± 0.029	12.782 ± 0.024	13.292 ± 0.031
WISE- <i>W3</i>	12.662	13.089	12.72 ± 0.32	13.222

de Haute-Provence (OHP, France) to characterize *Kepler* candidates. We mainly focus on the brightest stars (*Kepler* magnitude $K_p < 14.7$) harboring close-in giant planet candidates. This has allowed us to identify and characterize several new transiting planets (Santerne et al. 2011a, 2011b; Bonomo et al. 2012; Deleuil et al. 2014), as well as more massive companions and false positives (Ehrenreich et al. 2011; Bouchy et al. 2011; Santerne et al. 2012; Díaz et al. 2013; Moutou et al. 2013). We are extending our on-going SOPHIE program on KOIs characterization with the HARPS-N spectrograph at the *Telescopio Nazionale Galileo* (TNG, La Palma, Spain), taking advantage of its higher radial-velocity accuracy for fainter targets. Our observation strategy with HARPS-N complements SOPHIE observations in three ways. First, we use HARPS-N to follow KOIs for which our SOPHIE data provides only a detection hint or an upper limit on the planetary mass, but with a precision preventing firm conclusion and accurate characterization. Second, we use HARPS-N to follow KOIs fainter than the limit $K_p = 14.7$ adopted in the SOPHIE sample. Third, we also use HARPS-N to follow KOIs with shallower transits than those observed with SOPHIE. As part of that HARPS-N program, we previously reported (Hébrard et al. 2013a) the characterization of the two new transiting planets KOI-200b and KOI-889b (afterwards named Kepler-74b and Kepler-75b by the *Kepler* Team); these planets complied with the conditions of detection hint and faintness, respectively. Both are giant planets on 7.3- and 8.9-day orbits, but whereas KOI-200b has a mass of $0.68 \pm 0.09 M_{\text{Jup}}$, KOI-889b is a massive planet of $9.9 \pm 0.5 M_{\text{Jup}}$. These two planets were among the first ones to be detected with HARPS-N. HARPS-N has also been used to measure the mass of the Earth-sized planets Kepler-78b (Pepe et al. 2013; see also Sanchis-Ojeda et al. 2013 and Howard et al. 2013) and Kepler-10b,c (Dumusque et al. 2014), and also to study obliquities in planetary systems (Covino et al. 2013; Esposito et al. 2014; Santerne et al. 2014; Bourrier & Hébrard 2014; Lopez-Morales et al. 2014), to show that the metal-poor star HIP 11952 does not harbor giant planets (Desidera et al. 2013), and to study the planetary system around XO-2S (Desidera et al. 2014).

Here we present the characterization of four new transiting planets with HARPS-N, namely KOI-188b, KOI-195b, KOI-192b, and KOI-830b. The IDs and coordinates of the four planet-host stars are given in Table 1, which also presents their spectral

energy distributions (SEDs) from magnitudes at different wavelengths. KOI-192 was in the SOPHIE sample, but its nature was not established and only an upper mass of $0.6 M_{\text{Jup}}$ could be put on the transiting object if actually it was a planet (Santerne et al. 2012). The other three objects are fainter than the magnitude limit of the SOPHIE sample. We also report here the identification of KOI-219.01 as a false positive, which is in our third sample which includes shallower transit candidates.

We describe the photometric and spectroscopic observations of the targets in Sect. 2, the analysis of the datasets in Sect. 3, and the results and their discussion in Sect. 4.

2. Observations and data reduction

2.1. Photometric detection with *Kepler*

The five targets were observed by *Kepler* since the beginning of the mission in May 2009, and were identified by Borucki et al. (2011a, 2011b) and Batalha et al. (2013) as hosting single periodic transits with periods of a few days and depths characteristic of giant planets. No transits with different periods were detected in any of the light curves, so there are no signs of multiple transiting systems.

The *Kepler* photometry was acquired in long-cadence data (LC, one point per 29.42 minutes). Short-cadence data (SC, one point per 58 seconds) are also available for KOI-188, KOI-195, and KOI-192. Both LC and SC were used in our present analyses. We used the light-curve of quarters Q1 to Q17 reduced by the Photometric Analysis *Kepler* pipeline that accounts for barycentric, cosmic ray, background, and so-called argabrightening corrections (Jenkins et al. 2010), publicly available from the MAST archive (<http://archive.stsci.edu/kepler>). The light curves clearly present transits with depths of about 1 %.

They also show smooth variations of the flux which could be due, at least partially, to inhomogeneities of the stellar surfaces (spots, plages, etc) modulated with the rotation of the stars. The stronger variations are seen on KOI-188 with an amplitude up to 2500 ppm in normalized flux. The variations are weaker for the three other targets, with amplitudes up to 700, 500, and 400 ppm for KOI-195, KOI-192, and KOI-830, respectively. We used Lomb-Scargle periodograms and autocorrelations of the light curves to attempt detections of stellar rotation periods. In the case of KOI-188, we obtained different rotation periods in

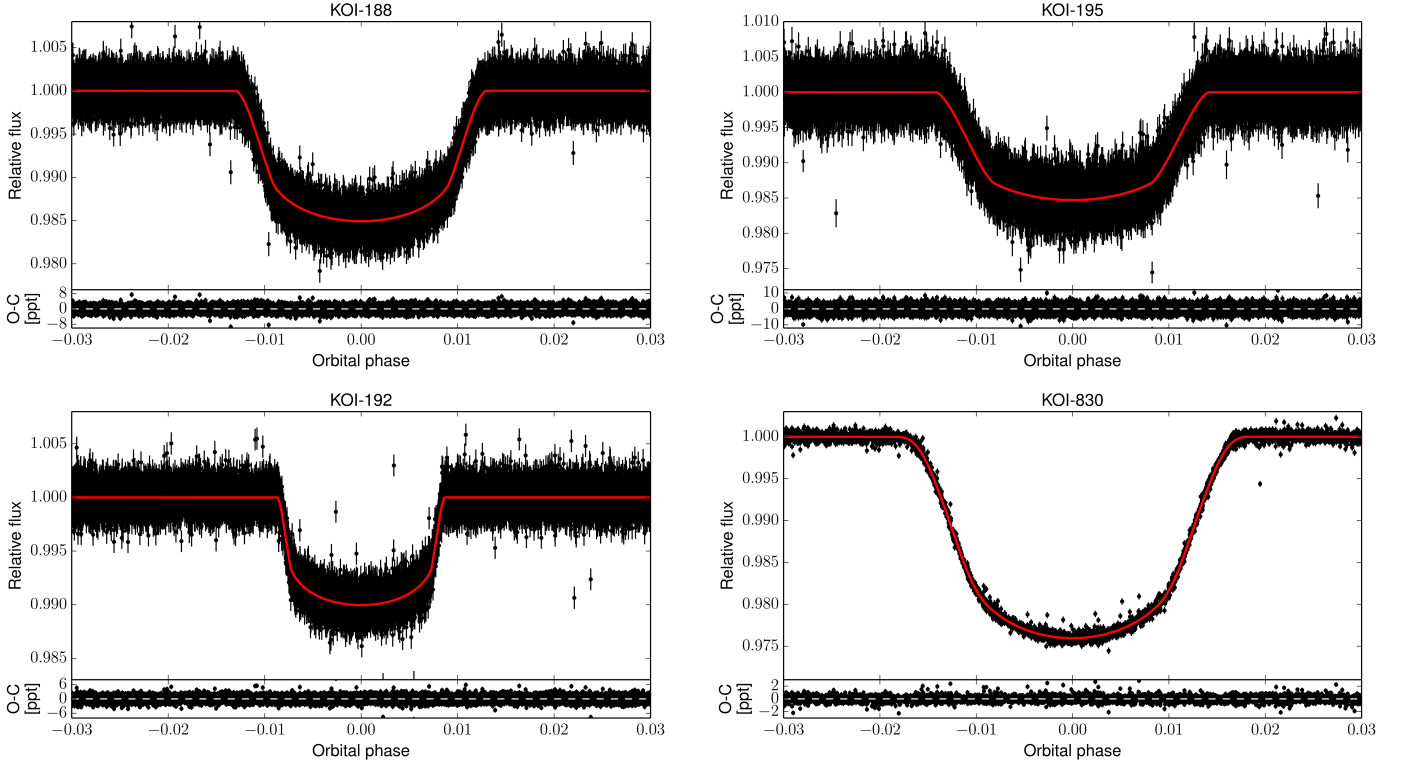


Fig. 1. *Kepler* photometric data of the four planet-host stars. On each plot the upper panel shows the phase-folded light-curve (black dots with $1\text{-}\sigma$ error bars) over-plotted with the best model (red line; see Sect. 3.2), and the lower panel shows the residuals. The models fit together the photometric data, the radial velocities, and the spectral energy distribution (Table 3 and Fig. 2). The parameters of the fits are reported in Tables 4 and 5. Only *Kepler* short-cadence data are plotted here for KOI-188, KOI-195, and KOI-192, but long-cadence data are also used in the analysis of these three systems. No short-cadence data are available for KOI-830, whose long-cadence data are plotted here.

a range between 10 and 40 days, depending on the section of the light curve we used. We thus conclude that the signal is not significant enough to allow a reliable stellar rotation period to be derived. The signal is even less significant for the three other targets. We note that Walkowicz & Basri (2013) reported $P_{\text{rot}} = 35.00 \pm 8.32$ days from the *Kepler* light curve of KOI-188, the large uncertainty probably reflecting the weaknesses of the signal. They do not report any detection for the other three targets.

Before modeling the transits, we normalized fragments of the light curves by fitting an out-of-transit parabola, first without accounting for contamination. Since the *Kepler* spacecraft rotates four times a year, the crowding values are different between seasons. We thus produced four crowding-uncorrected detrended light curves for each target, one per season. This allowed us to account for differential crowding values, noises, and out-of-transit fluxes in the transit modeling and in the final error budget (see Sect. 3.2). Figure 1 shows the corresponding phase-folded light curves, once normalized and corrected for crowding.

2.2. Radial velocities

2.2.1. Pre-screening with SOPHIE

Although we observed KOI-830 only with HARPS-N, we first observed the other four targets with SOPHIE, the fiber-fed, echelle spectrograph mounted at the focus of the 1.93 m OHP telescope and dedicated to high-precision radial velocity mea-

surements (Perruchot et al. 2008; Bouchy et al. 2009, 2013). Even if the precision is lower than the HARPS-N measurements for such faint targets, SOPHIE measurements can reveal large radial velocity variations corresponding to transiting stars, brown dwarfs, or massive planets, which would not require HARPS-N to be characterized (see, e.g., Ehrenreich et al. 2011; Díaz et al. 2013; Moutou et al. 2013; Hébrard et al. 2013a). The observations were made in high-efficiency mode (resolution power $\lambda/\Delta\lambda = 40\,000$) using the slow read-out mode of the detector. The exposure times ranged between 20 and 55 minutes, allowing radial velocity accuracies between ± 20 and $\pm 50 \text{ m s}^{-1}$ to be reached (see Table 2).

The three observations of KOI-219 we secured with SOPHIE over a week in summer 2013 revealed a binary star. Depending on the observation, we detected two sets of barely resolved spectral lines separated by a few km s^{-1} , or a unique set of spectral lines that we interpreted as the superposition of the two sets being located at a similar radial velocity at that time. The corresponding radial velocities and bisector spans than we measured on these spectra show a clear correlation (Fig. 3), which means that the observed apparent radial velocity variations are mainly due to line profile variations rather than to Doppler shifts of the whole spectra. That candidate is thus likely to be an unresolved eclipsing stellar binary which is diluted in an associated triple system or in a foreground/background star. The full resolution of the binary scenario would require more observations and analyses, beyond the main scope of the present paper. Here we conclude that this transiting candidate is not a planet but a false pos-

Table 2. SOPHIE pre-screening measurements.

BJD _{UTC} -2 456 000	RV [km/s]	$\pm 1 \sigma$ [km/s]	Texp* [sec]	S/N**
<i>KOI-219:</i>				
472.4354	–	–	1800	10.8
475.5494	–	–	1800	14.3
478.4095	–	–	1800	14.0
<i>KOI-188:</i>				
150.4740	-45.514	0.036	2115	13.5
152.5412	-45.589	0.050	2513	11.6
<i>KOI-195:</i>				
153.4868	-78.976	0.046	1277	10.3
154.5257	-78.991	0.043	1946	13.8
<i>KOI-192:</i>				
754.4488	-24.346	0.024	2274	17.3
770.5076	-24.328	0.017	3304	17.4

* : duration of each individual exposure.

** : signal-to-noise ratio per pixel at 550 nm.

itive, so we did not pursue the observation of KOI-219 with the higher precision of HARPS-N. This illustrates the benefits that could be obtained for the follow-up of transiting planet candidates from coordinated observations secured with two spectrographs with different sensitivities, precisions, and accessibilities as SOPHIE and HARPS-N. Similar cases of diluted eclipsing binaries revealed with SOPHIE among the KOIs were presented by Santerne et al. (2012).

The SOPHIE observations of the three remaining candidates did not reveal any false positives. Two successive observations were performed in July 2011 for KOI-192, then in August 2012 for KOI-188 and KOI-195. For the three targets, the two observations were separated by a few days and made at quadratures, i.e., at $\sim P/4$ before and after a transit, P being the period of the transits. This allows any radial velocity shift to be highest if the orbit of the transiting object is circular, which is a reasonable assumption given the short periods considered here. The SOPHIE radial velocities are plotted in the three upper panels of Fig. 2 and show no significant variations. The largest variation is observed in the case of KOI-188, but it is not significant according to the error bars.

2.2.2. Accurate radial velocities with HARPS-N

Since these three targets harbor no evident massive transiting objects, we observed them with HARPS-N in order to increase the radial velocity accuracy by comparison to SOPHIE. We directly observed KOI-830 with HARPS-N, without initial pre-screening selection with SOPHIE. The HARPS-N spectrograph (Cosentino et al. 2012) is similar to SOPHIE, but it allows better radial velocity accuracy to be reached, because of a more efficient stabilization system, and in particular in the case of our faint targets because of the larger size of its telescope, the 3.58 m TNG. Its spectra provide a larger resolution power $\lambda/\Delta\lambda = 115\,000$. Our HARPS-N observations were secured in three different runs: five half-nights in August 2012, then four half-nights in September 2012, and finally six half-nights in July 2013. The three runs were made with the same instrument setup, with one exception: in 2012 we used the slow read-out mode of the detector, whereas in 2013 we used the fast read-out mode. The two 1''-wide optical-fiber apertures were used, the first one being on the target whereas the second one was on the nearby sky to estimate the moonlight pollution. The second aperture shows

Table 3. HARPS-N measurements.

BJD _{UTC} -2 456 000	RV† [km/s]	$\pm 1 \sigma$ [km/s]	bisect.‡ [km/s]	Texp* [sec]	S/N**
<i>KOI-188:</i>					
155.4892	-45.436	0.009	-0.038	2700	9.0
157.3792	-45.392	0.009	-0.013	2700	10.3
185.5019	-45.413	0.015	-0.016	2300	6.6
186.3782	-45.416	0.011	0.040	2300	7.7
489.5937	-45.439	0.012	-0.024	2300	9.2
490.6074	-45.439	0.018	-0.009	2100	6.5
491.6068	-45.361	0.009	-0.016	2700	11.4
492.6194	-45.400	0.014	-0.042	2700	8.1
493.6043	-45.433	0.007	-0.011	2700	13.7
494.6163	-45.407	0.019	-0.085	2700	6.5
<i>KOI-195:</i>					
156.5564	-78.800	0.012	-0.063	2700	10.2
157.4515	-78.860	0.016	0.005	2700	7.8
185.4254	-78.776	0.017	-0.081	2700	6.9
187.3785	-78.877	0.040	-0.159	2300	3.4
489.5329	-78.899	0.018	-0.033	2300	8.8
490.6366	-78.808	0.030	-0.030	2300	5.7
491.5386	-78.810	0.012	0.020	2700	11.9
492.6521	-78.869	0.020	0.047	2700	7.7
493.5702	-78.811	0.012	-0.025	2700	12.4
494.5483	-78.803	0.015	-0.015	2700	10.0
<i>KOI-192:</i>					
156.3892	-23.961	0.007	-0.008	2700	16.9
159.4238	-23.935	0.010	0.007	2700	11.6
185.5580	-23.953	0.013	0.070	1400	9.5
188.3849	-23.956	0.018	-0.051	2700	6.4
490.5791	-23.912	0.014	-0.002	2300	12.0
491.5727	-23.908	0.008	0.006	2700	18.5
492.5558	-23.921	0.008	-0.002	2700	17.7
493.6969	-23.956	0.010	0.004	2500	15.3
494.5825	-23.979	0.015	0.024	2700	11.4
<i>KOI-830:</i>					
157.4875	-21.368	0.016	-0.040	2700	5.8
489.6748	-21.152	0.026	-0.041	2100	4.6
491.6366	-21.475	0.019	-0.037	2100	6.2
492.6819	-21.323	0.048	-0.250	1800	2.5
493.7245	-21.103	0.027	0.016	1800	4.5
494.7325	-21.432	0.060	-0.065	1300	2.4

† : radial velocities include season offsets δV_0 (see Sect. 2.2.2).

‡ : bisector spans; error bars are twice those of the RVs.

* : duration of each individual exposure.

** : signal-to-noise ratio per pixel at 550 nm.

detectable moonlight only on some exposures secured at the end of the last three half-nights of the 2013 run. Nevertheless, the apparent radial velocity of the Moon each time was far from that of the targets and weak enough to avoid a significant effect on the radial velocity measurement.

As in the case of SOPHIE above, the HARPS-N spectra were extracted from the detector images with the standard DRS pipeline, which includes localization of the spectral orders on the 2D images, optimal order extraction, cosmic-ray rejection, corrections of flat-field, and wavelength calibration with thorium lamp exposures made during the afternoon. Then the spectra passed through weighted cross-correlation with numerical masks following the method described by Baranne et al. (1996) and Pepe et al. (2002). Because the blue part of the spectra has particularly low signal-to-noise ratios (S/N), we did not use the first 15 blue of the 70 available orders for the cross-correlation. All the exposures provide a well-defined, single peak in the cross-correlation function (CCF), whose Gaussian

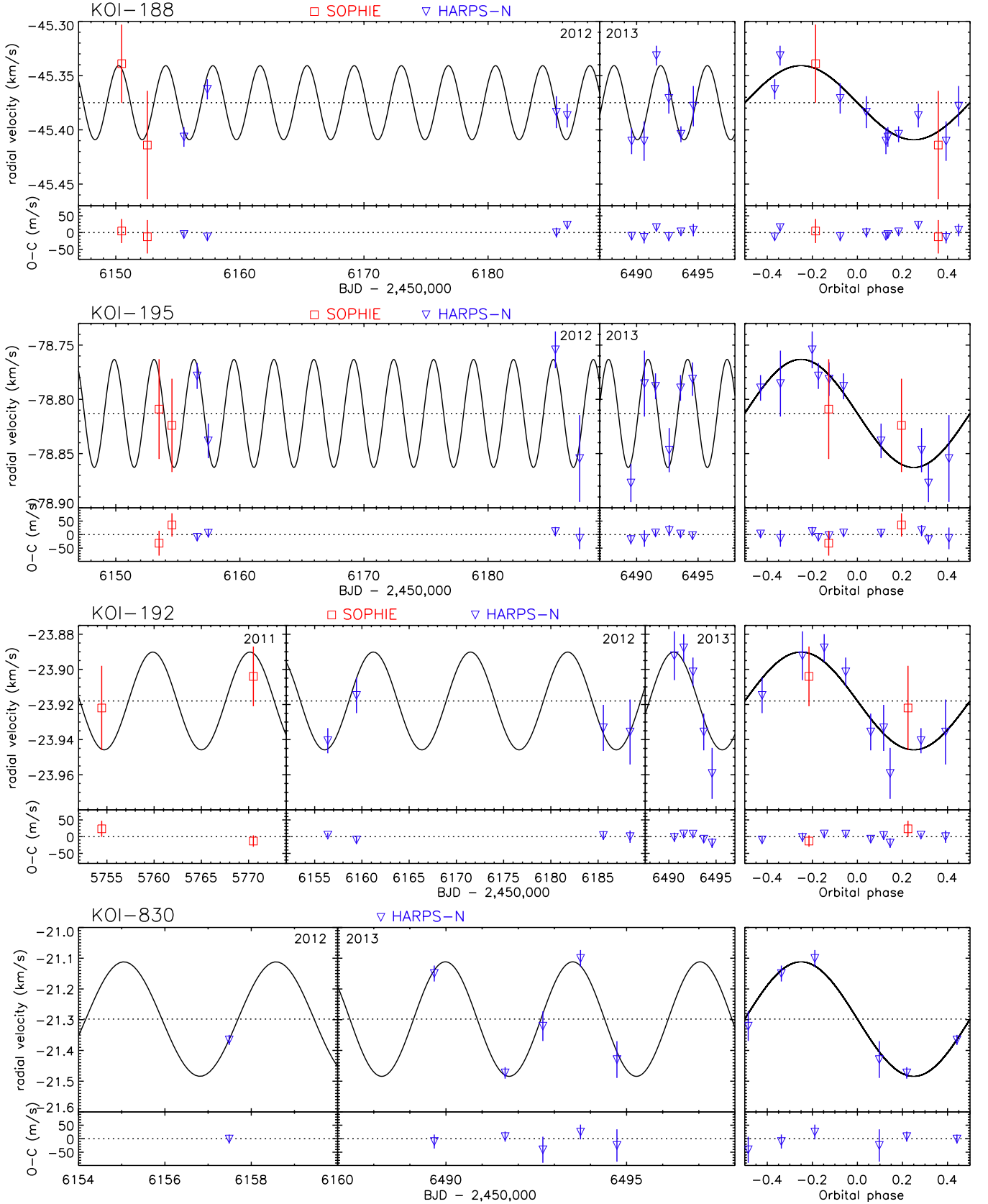


Fig. 2. Radial velocities of the four planet-host stars, from HARPS-N (blue) and SOPHIE (red), and 1- σ error bars. On each of the four plots, the left panel shows the radial velocities as a function of time, the right panel shows the phase-folded data, the upper panel shows the data over-plotted with the best circular model (black line), and the lower panel shows the residuals. The parameters of the fits are given in Tables 4 and 5.

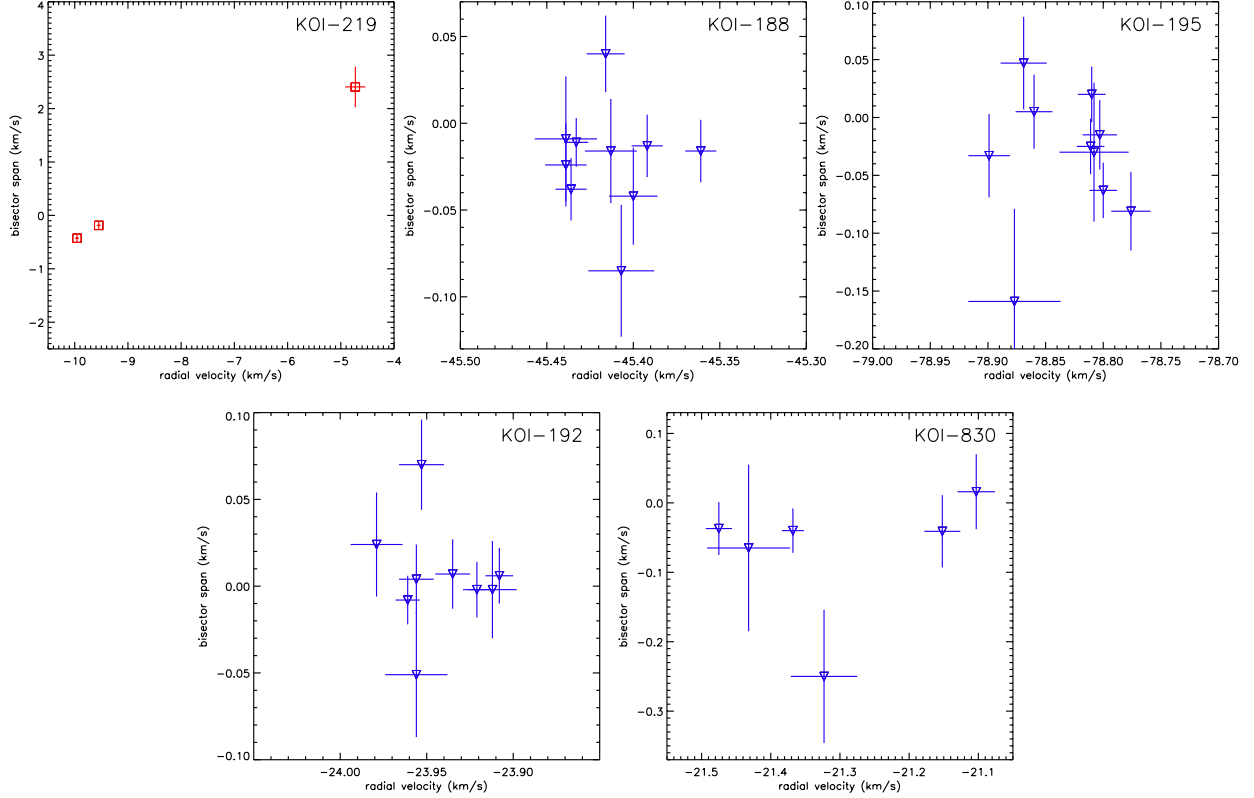


Fig. 3. Bisector span as a function of the radial velocities with $1\text{-}\sigma$ error bars for the five targets. The ranges have the same extents in the x - and y -axes on each figure. A correlation between bisector spans and radial velocities is clearly detected with SOPHIE on KOI-219, showing that the transiting planet candidate is a false positive. For the other four targets, the HARPS-N measurements show no significant variations or trends of the bisector spans.

fits allow the radial velocities to be measured together with their associated uncertainties. The bisector spans of each CCF were also measured.

The HARPS-N measurements are reported in Table 3 and are plotted in Fig. 2. As seen on the phase-folded curves, for each of the four targets the radial velocity variations are in phase with the *Kepler* ephemeris and have semi-amplitudes of ~ 30 , ~ 50 , ~ 30 , and ~ 200 m/s for KOI-188, KOI-195, KOI-192, and KOI-830, respectively. This corresponds to Saturn-mass companions for the first three objects, and to a Jupiter-mass companion for the fourth one.

To fit the data we have to use an offset (or a drift) in addition to the Keplerian model adjusted to the *Kepler* ephemeris. The offset being similar for the four targets (on the order of -20 m/s/yr), this clearly indicates its origin is instrumental and not the signature of additional, long period companions in the systems. Exactly the same spectral orders were used in the cross-correlation, which in addition was done using the same version of the DRS pipeline (HARPN_3.6), so there are no obvious reasons due to the reduction for such systematic shift. We found no systematic differences in the characteristics of the 2012 and 2013 measurements, e.g., concerning their typical accuracies or the moonlight pollution. The HARPS-N detector was changed between our 2012 and 2013 runs, but no shifts as large as the one we detect here were seen in other targets observed both before and after that modification (F. Pepe, private communication). Another possibility is the charge transfer inefficiency (CTI) of the detector, which could induce radial velocity shifts at low S/N (e.g., Bouchy et al. 2008). This effect is not corrected

on our data and is likely to be different between the 2012 and 2013 HARPS-N detectors. However, our observations of a given target present various, low S/N, without correlations between the S/N and the radial velocity residuals after the Keplerian fits. So the CTI effect seems to be low, for both the 2012 and 2013 detectors. The only difference we identify between our datasets is the read-out modes of the detector, which was the slower of the two 2012 runs, and the faster in 2013. If this really is the cause of the instrumental shift, this could be tested in the future by additional, dedicated tests on constant stars. So in the rest of the paper we assume there is an instrumental shift δV_0 between our 2012 and 2013 radial velocity measurements, which is computed in Sect. 3.1. The data in Table 3 and Figs. 2 and 3 are corrected for that shift. As the fast read-out mode is the standard one, we used the 2013 data as the reference ones. The data secured in slow read-out mode are redshifted in comparison to those secured in fast read-out mode, so we corrected by shifting the first ones toward the blue.

The cross-correlation function bisector spans show neither significant variations nor trends as a function of radial velocity (Fig. 3). This is the same for the width of the CCFs. This agrees with the interpretation of the measured radial velocity variations as only being due to Doppler shifts instead of line profile deformations. Similarly, the radial velocities obtained using different stellar masks (G2, K0, or K5) produce variations with similar amplitudes. So there is no evidence that the variations could be explained by scenarios implying blended stars. We have chosen the numerical mask that produced the best fits, i.e., the less dispersed residuals around the Keplerian fits: there are the K5-, G2-,

K0-, and K0-type masks for KOI-188, KOI-195, KOI-192, and KOI-830, respectively.

All these observations allow us to conclude that the four targets harbor transiting giant planets, and so hereafter we do not consider them anymore as candidates but as planets, which we now designate as KOI-188b, KOI-195b, KOI-192b, and KOI-830b.

3. System characterization

3.1. Spectral analysis of the host stars

We analyzed the co-added individual HARPS-N spectra of the four planet-host stars. The signal-to-noise ratios of the co-added spectra are 160, 120, 220, and 60 per resolution element at 550 nm in the continuum for KOI-188, KOI-195, KOI-192, and KOI-830, respectively. The projected rotational velocity $v \sin i_*$ was determined from a set of isolated spectral lines. None of the stars is rapidly rotating.

We performed the spectral analysis using the iterative spectral synthesis package VWA (versatile wavelength analysis). As described in detail by Bruntt et al. (2010) and references therein, the atmospheric parameters T_{eff} , $\log g_*$, and $[\text{Fe}/\text{H}]$ were derived from tens of Fe I and Fe II weak lines carefully selected, the exact number of lines depending on the signal-to-noise ratio of the spectra. Ionization and excitation equilibria were imposed, as well as a zero slope between the abundances given by individual lines and their equivalent widths. As a verification, we also derived the surface gravity from the Ca I pressure-sensitive line at 612.2 nm. These parameters are used below (Sect. 3.2) to derive the fundamental parameters of the four stars (mass, radius, and age) from the distribution of stellar density derived from the transit modeling and from the comparison of the location of the star in the H-R Diagram with evolution tracks. As the S/N of the co-added HARPS-N spectrum of KOI-830 is lower than that of the other objects, this implies less accurate derived stellar parameters for that star. This is particularly the case for $v \sin i_*$ and $\log g_*$ which are difficult to measure with the available data, and for which we chose to adopt conservative error bars.

3.2. Parameters of the planetary systems

The normalized *Kepler* light curves were fitted together with the HARPS-N radial velocities by a transit model using the EBOP code (Etzel 1981) and a Keplerian model. For the combined fits we used the PASTIS code (Díaz et al. 2014), following the procedures used, e.g., by Díaz et al. (2013) and Hébrard et al. (2013a). The analysis also includes the fit of the SED (from magnitudes reported in Table 1) and stellar evolution tracks to determine coherent stellar parameters. The distances of the four stars were determined by comparing the SED with an interpolated grid of synthetic spectra from the PHOENIX/BT-Settl library (Allard et al. 2012), corrected for the interstellar extinction. We used four different stellar evolution tracks as input for the stellar parameters of each target: StarEvol (Lagarde et al. 2012; A. Palacios, private communication), Dartmouth (Dotter et al. 2008), Parsec (Bressan et al. 2012), and Geneva (Mowlavi et al. 2012).

We used an oversampling factor of ten when comparing the model with the *Kepler* long-cadence light curves to account for their long integration time (Kipping 2010; Kipping & Bakos 2011). As explained above (see Sect. 2.2.2), we allow a free radial velocity shift between the 2012 and 2013 HARPS-N data in order to correct for the season offset δV_0 . For each *Kepler* light curve we included the out-of-transit flux and the contami-

nation factor as free parameters. Contamination factors reported in the KIC (Brown et al. 2011) have been shown to be incorrect in some cases (see, e.g., KOI-205; Díaz et al. 2013) so we chose to fit them instead of adopting the KIC values. Similarly, we left the limb-darkening coefficients free to vary within a Gaussian prior centered on the estimated values. We also account for additional sources of Gaussian noise in the light curves, radial velocities, and SED by fitting a jitter value to each dataset. This is especially appropriate for the *Kepler* data since the star is located on different CCDs each season. For each target we performed both fits with eccentric or circular orbits. In none of them did we detect a significant eccentricity. In the case of KOI-192 we obtained a weak constraint on the eccentricity so we adopted the conservative values of the parameters obtained with the eccentric fit. For the three other targets we constrained the eccentricities to low values so we adopted the parameters obtained from the circular fits; we discuss that assumption below. We conservatively adopted the 99 % upper limits for the eccentricity of the four systems.

For each of the four systems and datasets we thus have 25 free parameters (27 for eccentric fits), which we have fitted using a Metropolis-Hasting Markov chain Monte Carlo (MCMC) algorithm (e.g., Tegmark et al. 2004) with an adaptive step size (Ford 2006). To better sample the posterior distribution in the case of non-linear correlations between parameters, we applied an adaptive principal component analysis to the chains and jumped the parameters in an uncorrelated space (Díaz et al. 2014). For most of the parameters of the MCMC we used non-informative priors (uniform or Jeffreys distributions). Exceptions are the stellar parameters T_{eff} , $[\text{Fe}/\text{H}]$, and ρ_* derived from the above spectral analysis (Sect. 3.1), and the orbital periods and phases of the planets for which we used as priors the *Kepler* values with error bars increased by a factor of 100 to avoid biases. We chose the factor 100 as a conservative one by comparison with smaller factors which provide similar results. We finally obtained orbital periods in perfect agreement with the *Kepler* values. All the priors of the final fits are listed in the Table 6 available online.

The systematic uncertainties due to the stellar evolution model are not easy to quantify. In order to attempt to take these uncertainties into account in our final results, the MCMC chains were calculated using the four different sets of models in equal proportions. This allows possible discrepancies between stellar evolution models to be taken into account in the MCMC chains and thus in our final results, while including the state-of-the-art knowledge about stellar evolution models. Some additional uncertainties might remain, as it could be defaults common to all stellar evolution models.

Each system was analyzed with 4×10 chains (one per stellar evolution track) leading to a total of 4×10^7 steps. Each chain was started at random points drawn from the joint prior. All chains converged to the same solution. For each target we computed the correlation length of the converged sub-chains before thinning them. We finally merged the thinned chains, which left us with a total of more than 1000 independent samples of the posterior distribution for each target.

The models are shown in Figs. 1 and 2, and the 68.3 % confidence intervals (corresponding to $1-\sigma$ intervals assuming Gaussian distributions) are listed in Tables 4 and 5. We did not find any significant jitter to add to radial velocities, and the dispersion of the residuals around the Keplerian fit are slightly smaller than the error bars on the radial velocities. This suggests the estimated uncertainties on the HARPS-N radial velocities could be slightly overestimated. The four measured values

Table 4. Parameters of the transiting hot Saturns KOI-188b and KOI-195b and their host stars.

	KOI-188	KOI-195
<i>Ephemerides and orbital parameters:</i>		
Planet orbital period P [days]	$3.79701816 \pm 0.00000019$	$3.21751883 \pm 0.00000019$
Transit epoch T_0 [BJD – 2 454 900]	66.508785 ± 0.000039	66.631964 ± 0.000047
Orbital eccentricity e (99 % upper limit)	< 0.33	< 0.18
Orbital inclination i_p [°]	87.02 ± 0.08	85.74 ± 0.06
Transit duration T_{1-4} [hours]	2.353 ± 0.006	2.191 ± 0.010
Impact parameter b	0.602 ± 0.012	0.718 ± 0.007
<i>Transit-related parameters:</i>		
System scale a/R_*	11.60 ± 0.08	9.67 ± 0.06
Radius ratio $k = R_p/R_*$	0.1168 ± 0.0008	0.1221 ± 0.0013
Linear limb-darkening coefficient u_a	0.53 ± 0.07	0.43 ± 0.20
Quadratic limb-darkening coefficient u_b	0.15 ± 0.12	0.20 ± 0.27
<i>RV-related parameters:</i>		
Semi-amplitude K [m s ⁻¹]	34 ± 10	50 ± 10
HARPS-N systemic radial velocity V_0 [km s ⁻¹]	-45.404 ± 0.009	-78.835 ± 0.010
HARPS-N season offset δV_0 [m s ⁻¹]	29 ± 18	22 ± 20
O-C residuals [m s ⁻¹]	11.5	8.6
<i>Data-related parameters:</i>		
Kepler season 0 contamination [%]	4.50 ± 0.40	5.78 ± 0.42
Kepler season 1 contamination [%]	4.30 ± 0.43	5.78 ± 0.43
Kepler season 2 contamination [%]	4.42 ± 0.41	6.16 ± 0.45
Kepler season 3 contamination [%]	4.28 ± 0.40	6.48 ± 0.44
Kepler season 0 jitter LC [ppm]	121 ± 11	204 ± 10
Kepler season 0 jitter SC [ppm]	310 ± 46	66 ± 59
Kepler season 1 jitter LC [ppm]	99 ± 12	246 ± 9
Kepler season 1 jitter SC [ppm]	156 ± 85	–
Kepler season 2 jitter LC [ppm]	240 ± 9	315 ± 11
Kepler season 2 jitter SC [ppm]	36 ± 33	210 ± 9
Kepler season 3 jitter LC [ppm]	164 ± 10	237 ± 15
Kepler season 3 jitter SC [ppm]	46 ± 41	98 ± 69
HARPS-N jitter [m s ⁻¹]	0.014 ± 0.015	0.011 ± 0.015
SED jitter [mag]	0.065 ± 0.026	0.084 ± 0.029
<i>Spectroscopic parameters:</i>		
Effective temperature T_{eff} [K]	5170 ± 70	5725 ± 90
Metallicity [Fe/H] [dex]	0.24 ± 0.11	-0.21 ± 0.08
Stellar rotational velocity $v \sin i_*$ [km s ⁻¹]	3 ± 1	3 ± 1
Spectral type	K1V	G1V
Stellar surface gravity $\log g_*$ [g cm ⁻²]	4.50 ± 0.15	4.50 ± 0.15
<i>Stellar physical parameters from combined analysis:</i>		
Stellar surface gravity $\log g_*$ [g cm ⁻²]	4.535 ± 0.010	4.471 ± 0.011
Stellar density ρ_* [g cm ⁻³]	1.448 ± 0.030	1.170 ± 0.023
Star mass M_* [M _⊙]	0.93 ± 0.05	0.91 ± 0.06
Star radius R_* [R _⊙]	0.86 ± 0.02	0.92 ± 0.02
Age of the star [Gyr]	5 ± 4	6 ± 4
Luminosity of the star $\log(L/L_⊙)$	-0.323 ± 0.031	-0.089 ± 0.042
Distance of the system [pc]	650 ± 20	880 ± 30
Interstellar extinction $E(B - V)$ [mag]	0.024 ± 0.022	0.055 ± 0.030
<i>Planetary physical parameters from combined analysis:</i>		
Orbital semi-major axis a [AU]	0.0464 ± 0.0008	0.0414 ± 0.0010
Planet mass M_p [M _{Jup}]	0.25 ± 0.08	0.34 ± 0.08
Planet radius R_p [R _{Jup}]	0.978 ± 0.022	1.09 ± 0.03
Planet density ρ_p [g cm ⁻³]	0.27 ± 0.07	0.26 ± 0.06
Planetary equilibrium temperature T_p [K]	1070 ± 15	1300 ± 20

of the instrumental offsets between 2012 and 2013 provide the average shift $\delta V_0 = 21.6 \pm 10.2$ m/s. The fact that data secured in slow read-out mode are redshifted by this offset value in comparison to those secured in fast read-out mode can be checked by dedicated tests. We did not use the SOPHIE radial velocities in the final fit because their error bars do not allow significant constraints to be put by comparison to the more accurate HARPS-N radial velocities. Still, the SOPHIE data are plotted in Fig. 2 for illustration after their systemic radial velocity was determined from χ^2 variations (we found -45.551 ± 0.035 , -78.883 ± 0.022 ,

and -24.342 ± 0.018 km s⁻¹ for KOI-188, KOI-195, and KOI-192, respectively).

The out-of-transit fluxes were found around unity with typical uncertainties of 10 ppm. The contamination factors found for short- and long-cadence data agree for each season of each target. We found values similar to those tabulated in the KIC, except for KOI-195 where our fitted contamination factors were systematically larger than the KIC ones. The jitters found on the photometry are classical for *Kepler* data. Our fitted limb-darkening coefficients are compatible within 1σ with the expected values from Claret & Bloemen (2011). None of the

Table 5. Parameters of the transiting planets KOI-192b and KOI-830b and their host stars.

	KOI-192	KOI-830
<i>Ephemerides and orbital parameters:</i>		
Planet orbital period P [days]	10.2909940 ± 0.0000011	$3.52563254 \pm 0.00000015$
Transit epoch T_0 [BJD – 2 454 900]	70.02207 ± 0.00009	103.048008 ± 0.000032
Orbital eccentricity e (99 % upper limit)	< 0.57	< 0.22
Orbital inclination i_p [°]	89.50 ± 0.45	89.36 ± 0.43
Transit duration T_{1-4} [hours]	4.286 ± 0.009	2.614 ± 0.007
Impact parameter b	0.09 ± 0.07	0.13 ± 0.09
<i>Transit-related parameters:</i>		
System scale a/R_*	14.2 ± 2.1	11.65 ± 0.10
Radius ratio $k = R_p/R_*$	0.0913 ± 0.0003	0.1384 ± 0.0010
Linear limb-darkening coefficient u_a	0.450 ± 0.017	0.584 ± 0.017
Quadratic limb-darkening coefficient u_b	0.13 ± 0.04	0.10 ± 0.06
<i>RV-related parameters:</i>		
Semi-amplitude K [m s ⁻¹]	29.8 ± 9.1	188 ± 26
HARPS-N systemic radial velocity V_0 [km s ⁻¹]	-23.938 ± 0.010	-21.302 ± 0.024
HARPS-N season offset δV_0 [m s ⁻¹]	20 ± 18	3 ± 31
O-C residuals [m s ⁻¹]	8.0	13.4
<i>Data-related parameters:</i>		
Kepler season 0 contamination [%]	3.32 ± 0.44	7.68 ± 0.52
Kepler season 1 contamination [%]	3.61 ± 0.42	7.24 ± 0.52
Kepler season 2 contamination [%]	3.16 ± 0.43	7.07 ± 0.52
Kepler season 3 contamination [%]	3.67 ± 0.44	7.46 ± 0.51
Kepler season 0 jitter LC [ppm]	150 ± 8	226 ± 10
Kepler season 0 jitter SC [ppm]	230 ± 50	–
Kepler season 1 jitter LC [ppm]	127 ± 9	153 ± 13
Kepler season 1 jitter SC [ppm]	241 ± 65	–
Kepler season 2 jitter LC [ppm]	101 ± 10	182 ± 12
Kepler season 2 jitter SC [ppm]	291 ± 35	–
Kepler season 3 jitter LC [ppm]	122 ± 9	127 ± 17
Kepler season 3 jitter SC [ppm]	345 ± 28	–
HARPS-N jitter [m s ⁻¹]	0.008 ± 0.012	0.026 ± 0.024
SED jitter [mag]	0.056 ± 0.025	0.065 ± 0.029
<i>Spectroscopic parameters:</i>		
Effective temperature T_{eff} [K]	5800 ± 70	5150 ± 100
Metallicity [Fe/H] [dex]	-0.19 ± 0.07	0.09 ± 0.17
Stellar rotational velocity $v \sin i_*$ [km s ⁻¹]	3 ± 1	2 ± 2
Spectral type	G2V	K1V
Stellar surface gravity $\log g_*$ [g cm ⁻²]	4.15 ± 0.15	5.0 ± 0.4
<i>Stellar physical parameters from combined analysis:</i>		
Stellar surface gravity $\log g_*$ [g cm ⁻²]	4.14 ± 0.12	4.571 ± 0.011
Stellar density ρ_* [g cm ⁻³]	0.4 ± 0.2	1.704 ± 0.041
Star mass M_* [M _⊙]	0.96 ± 0.06	0.87 ± 0.05
Star radius R_* [R _⊙]	1.35 ± 0.20	0.80 ± 0.02
Age of the star [Gyr]	7 ± 4	5 ± 4
Luminosity of the star $\log(L/L_⊙)$	0.29 ± 0.13	-0.39 ± 0.05
Distance of the system [pc]	1100 ± 150	720 ± 25
Interstellar extinction $E(B - V)$ [mag]	0.022 ± 0.019	0.040 ± 0.037
<i>Planetary physical parameters from combined analysis:</i>		
Orbital semi-major axis a [AU]	0.091 ± 0.010	0.0433 ± 0.0009
Planet mass M_p [M _{Jup}]	0.29 ± 0.09	1.27 ± 0.19
Planet radius R_p [R _{Jup}]	1.23 ± 0.21	1.08 ± 0.03
Planet density ρ_p [g cm ⁻³]	0.16 ± 0.14	1.02 ± 0.15
Planetary equilibrium temperature T_p [K]	1100 ± 70	1070 ± 25

light curves show the signature of planetary occultation at the secondary eclipse phase, as expected for relatively long-period planets such as these.

Finally, we investigated the bulk composition of the four planets using CEPAM (e.g., Guillot 2010). Planetary evolution models have been built following the method used in, e.g., Deleuil et al. (2014). The planets are assumed to be made of a central rocky core surrounded by a solar-composition envelope, but because they are irradiated giant planets, we also considered the cases where we dissipate a fraction (1%) of the incoming

stellar flux deep in the layers of the planet (for more details see, e.g., Guillot & Havel 2011; Almenara et al. 2013).

4. Results and discussions

The four new, transiting planets presented here are giant, close-in ones, with radii on the order of the Jupiter radius. They orbit slow-rotating stars located on the main sequence of the H-R Diagram. Their masses, periods, and radii are plotted in Fig. 4, and compared with other transiting planets as known in May 2014 according to the Exoplanet Orbit Database (exoplanets.org;

Wright et al. 2011). Our discussion below concentrates on giant planets mainly shown in these plots, and not on the low-mass and small-radius planets seen in the lower parts of the figures, which are clearly different from the four new planets presented here.

KOI-188b and KOI-195b are similar planets: their periods are $3.79701816 \pm 0.00000019$ and $3.21751883 \pm 0.00000019$ days, their masses 0.25 ± 0.08 and $0.34 \pm 0.08 M_{\text{Jup}}$, and their radii 0.978 ± 0.022 and $1.09 \pm 0.03 R_{\text{Jup}}$, respectively. The upper limits we found at 99 % on their eccentricities are 0.33 and 0.18. Eccentric fits provide similar results to the circular ones presented above, but with slightly increased uncertainties for some parameters such as the inclination or the a/R_* ratio. These close-in planets are expected to be circularized and to have eccentricities near 0. Indeed, even considering the higher bounds for their eccentricities, their circularization time-scales would be on the order of a few hundreds of Myrs, assuming a typical tidal dissipation efficiency of 10^6 and 10^7 for the planets and the stars, respectively (Matsumura et al. 2008). These two planets are similar to standard hot Jupiters but with lower masses, and could be called hot Saturns. Analogous planets include WASP-29b, WASP-39b, WASP-49b, HAT-P-19b, or CoRoT-25b (Hellier et al. 2010; Faedi et al. 2011; Lendl et al. 2012; Hartman et al. 2011; Almenara et al. 2013). As seen in the upper panel of Fig. 4, they are located in the low-mass range of the envelope where planets with shorter periods are rare. The lack of hot Saturns could be interpreted as a signature of evaporation of planets too close to their stars (e.g., Lecavelier des Étang 1997; Ehrenreich & Désert 2011). Both planets have particularly low densities on the order of $\rho_p = 0.25 \text{ g cm}^{-3}$ (lower panel of Fig. 4), making them favorable targets for atmospheric species detection in absorption. They could be considered as bloated hot Saturns as CoRoT-25b (Almenara et al. 2013), by comparison with planets with similar periods and masses but smaller radii and larger densities, such as CoRoT-8b (Bordé et al. 2010).

Both planets are slightly inflated compared to our own Saturn ($0.83 R_{\text{Jup}}$), which has an upper limit on its core mass estimated to be $20 M_{\oplus}$ (Guillot & Gautier 2014). Results from their interior modeling yield a core mass of $32 \pm 7 M_{\oplus}$ and $33^{+7}_{-4} M_{\oplus}$, for KOI-188b and KOI-195b and assuming dissipation. In fact, their estimated heavy elements content greatly depends on whether we dissipate stellar energy or not into the planets. With standard models (i.e., without dissipation), KOI-188b would have only $8^{+7}_{-4} M_{\oplus}$, and KOI-195b just $2^{+5}_{-2} M_{\oplus}$. Therefore, coreless models cannot be fully excluded from the possible solutions. However, many irradiated planets require a mechanism to dissipate external energy in their interior in order to explain their observed radius (Guillot & Gautier 2014). Thus, solutions taking into account some dissipation are preferred and should provide an upper-limit for the core-mass values given here. Interestingly, the uncertainties on the planetary mass of these two objects are large enough to allow for sub-Uranus mass planets at a 3- σ level. Our models can only go down as far as $0.04 R_{\text{Jup}}$ in masses, yet it is enough to put a lower limit on the masses of KOI-188b and KOI-195b based on these models: with dissipation, both should have masses larger than $\sim 0.1 M_{\text{Jup}}$ (2σ) in order to explain their measured radius and age, regardless of the amount of heavy elements we put in the core. However, with standard models we can put this same lower limit only on KOI-188b, if and only if we assume the planet has between about 5 and $10 M_{\oplus}$ of heavy elements.

Lastly, KOI-188b orbits an over-metallic K1V star, whereas KOI-195b orbits an under-metallic G1V star, which are the two main differences between the two systems. According to their

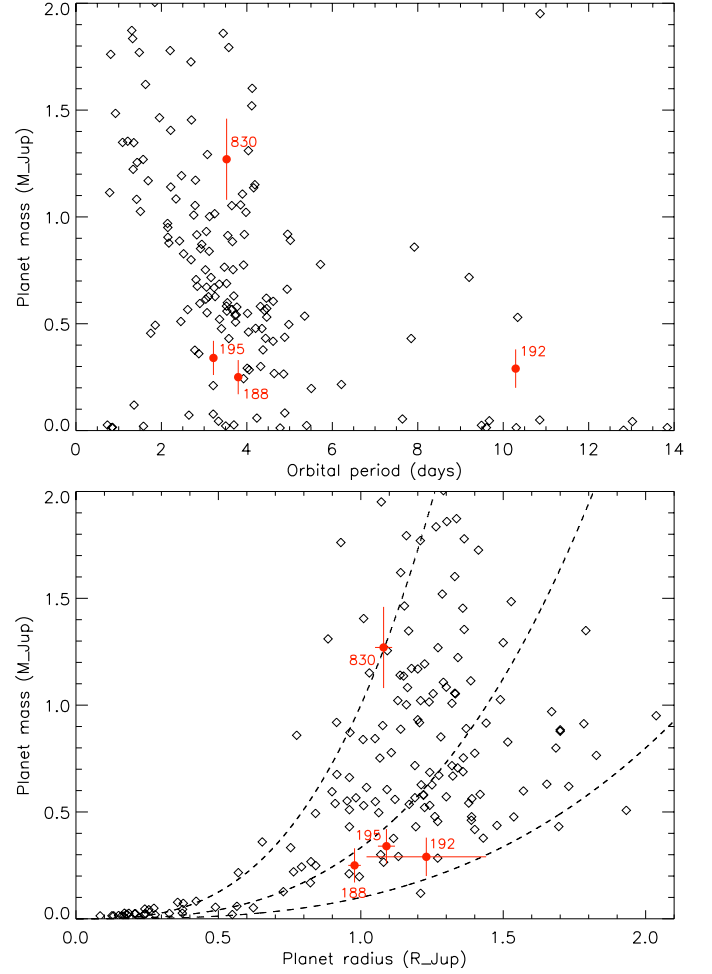


Fig. 4. Masses and orbital periods (top) and masses and radii (bottom) of the four new planets KOI-188b, KOI-195b, KOI-192b, and KOI-830b (red circles), compared to other known transiting, close-in planets (black diamonds). In the bottom panel, the three dashed curves show the Jupiter density, and 1/3 and 1/10 of that value (from left to right).

metallicity (Guillot et al. 2006), KOI-195b should likely have lighter core than KOI-188b. This would imply that, somehow, KOI-195b would dissipate the incoming stellar flux less effectively than KOI-188b could, implying differences in their atmospheric properties.

The planet KOI-192b orbits a G2V star. It has similar mass and radius ($0.29 \pm 0.09 M_{\text{Jup}}$ and $1.23 \pm 0.21 R_{\text{Jup}}$) to the two planets above, but its orbital period of 10.2909940 ± 0.0000011 days is longer. The measured mass agrees with the $0.6 M_{\text{Jup}}$ upper limit obtained with SOPHIE by Santerne et al. (2012). Our HARPS-N data did not allow us to significantly detect an eccentricity. We formally obtain $e = 0.35 \pm 0.11$ (corresponding to an argument of the pericenter $\omega = 93.6^\circ \pm 0.5^\circ$), but that value only stands on a few points, which could lead to a slight overestimation of the eccentricity in the case of correlated noise (see, e.g., Husnoo et al. 2011). Thus, we adopt the conservative 99 % upper limit $e < 0.57$. Eccentric orbits imply larger stellar and planetary radii than a circular orbit for KOI-192b, and lower corresponding densities. The large uncertainty on the stellar density results in a large uncertainty on its precise evolutionary status. As a consequence, among our four planet

host-stars, its radius and its inferred luminosity have the largest statistical uncertainties. As seen on the upper panel of Fig. 4, KOI-192b lies in a parameter space area (periods between 7 and 14 days and masses between 0.1 and 1.5 M_{Jup}) where only four other transiting planets are known, namely WASP-59b, CoRoT-4b, KELT-6b, and HAT-P-17b (Hébrard et al. 2013b; Moutou et al. 2008; Collins et al. 2014; Howard et al. 2012), whereas *Kepler* allowed numerous planets of lower masses to be detected at these orbital periods (seen at the bottom of the upper panel of Fig. 4). These four planets are all more massive than KOI-192b. The first three ones (WASP-59b, CoRoT-4b, and KELT-6b) have low-eccentricity orbits, whereas HAT-P-17b has an orbit with $e = 0.342 \pm 0.006$ and a long-period, cold Jupiter companion. The non-transiting planet HD 108147b (Pepe et al. 2002; Butler et al. 2006) has similar period and (sky-projected) mass, but its radius is unknown; its eccentricity is 0.498 ± 0.025 . Additional observations are mandatory to constrain the eccentricity of KOI-192b. Transiting planets in that long-period range are difficult to detect from ground-based photometry. The low mass also makes it difficult to detect in radial velocity on faint host stars, such as those observed by *Kepler* and CoRoT. So the scarcity of transiting planets with such orbital periods and masses could partly be due to observational biases. Radial velocity surveys detected a small amount of giant planets at intermediate orbital periods between about 10 and 100 days (the so-called period valley; see, e.g., Cumming et al. 2008; Mayor et al. 2011), but it is not as strong as the lack of giant planets on long periods seen in the upper panel of Fig. 4. Still, it remains difficult to distinguish true trends from observational biases.

We estimate the KOI-192b core-mass to be $16^{+22}_{-7} M_{\oplus}$ with dissipation models, and $1^{+4}_{-1} M_{\oplus}$ with standard ones. The larger relative error on these values are due to the larger error on the radius. This means that it is impossible to put any lower limit on the mass of KOI-192b based on the theoretical models we used. Despite its longer orbital period, the equilibrium temperature of KOI-192b is similar to that of KOI-188b because of the higher temperature of the host star. KOI-192b is cooler than the closer-in planet KOI-195b by about 200 K, but it could have a larger radius, which is not the expected trend.

Finally, KOI-830b has a mass of $1.27 \pm 0.19 M_{\text{Jup}}$ and a radius of $1.08 \pm 0.03 R_{\text{Jup}}$, corresponding to a density similar to that of Jupiter (lower panel of Fig. 4). Its short period of $3.52563254 \pm 0.00000015$ days makes it a standard hot Jupiter, which orbits a K1V star which could be slightly over-metallic. Its orbit is expected to be circularized, and we derived the 99 % upper limit $e < 0.22$. In its mass and radius range, there are no solutions from standard models, while dissipated-energy models provide a core-mass estimation of $45^{+25}_{-15} M_{\oplus}$. This is in line with what would be expected for a hot Jupiter orbiting around a metal-rich star. In comparison with the three other systems presented here, KOI-830 shows the larger disagreement between $(R_p/R_{\star})^2$ and the observed depth of the transits. The transit depth depends on $(R_p/R_{\star})^2$, but also on other parameters, including the limb darkening coefficients and the impact parameter. We note that KOI-830 and KOI-188 have similar limb-darkening coefficients but distinct impact parameters.

As for most known transiting planets, these four systems are not Darwin stable, and the ultimate fate of these close-in planets is to spiral into their stars (see, e.g., Hébrard et al. 2013a) although this evolution can be particularly slow for such low-mass planets. The characteristic timescales of tidal evolution depend on the tidal dissipation efficiency Q'_{\star} of their host star (Matsumura et al. 2010). Even considering a relatively efficient

dissipation of $Q'_{\star} = 10^6$, only KOI-830 would risk being engulfed before the end of the host's main-sequence.

5. Conclusions

We have presented the four new transiting, giant planets KOI-188b, KOI-195b, KOI-192b, and KOI-830b. They were detected thanks to *Kepler* photometry complemented by HARPS-N spectroscopic observations. The joined analysis of the datasets allowed us to characterize the four systems. When compared to the parameters initially derived by the *Kepler* Team from the initial *Kepler* light curves only (Brown et al. 2011; Borucki et al. 2011a, 2011b; Batalha et al. 2013), our derived parameters agree but are more accurate and robust. The identification of the planetary nature of the four objects as well as the planetary mass measurements are reported for the first time here. After the announcement of the present results, the *Kepler* Team gave to systems KOI-188, KOI-195, KOI-192, and KOI-830 the names Kepler-425, Kepler-426, Kepler-427, and Kepler-428, respectively (see Table 1).

These new secured planets improve the statistics of well-described planetary systems, in particular in the Saturn-mass regime where only few cases are known. They also provide new targets for follow-up studies on individual systems. Our observations also include a pre-screening with the SOPHIE spectrograph, which revealed KOI-219.01 to be a false positive. This confirms the fact that *Kepler* transiting candidates include targets which are actually not planets, in particular among the KOIs corresponding to close-in, giant companions. Follow-up studies are necessary both to establish the planetary nature of most of the transiting candidates identified from photometric surveys and to measure their mass.

Acknowledgements. This publication is based on observations collected with the NASA satellite *Kepler*, the HARPS-N spectrograph on the 3.58 m Italian *Telescopio Nazionale Galileo* (TNG) operated on the island of La Palma by the Fundación Galileo Galilei of the INAF (Istituto Nazionale di Astrofisica) at the Spanish Observatorio del Roque de los Muchachos of the Instituto de Astrofísica de Canarias (programs OPT13A.8 and OPT13B.30 from OPTICON common time allocation process for EC supported trans-national access to European telescopes), and the SOPHIE spectrograph on the 1.93 m telescope at *Observatoire de Haute-Provence* (CNRS), France (programs 11A.PNP.MOUT, 12A.PNP.MOUT, and 13A.PNP.MOUT). The authors particularly thank the *Kepler*, TNG, and OHP teams, whose work and expertise allowed these results to be obtained. This research has made use of the Extrasolar Planets Encyclopaedia (exoplanet.eu) and the Exoplanet Orbit Database (exoplanets.org). The research leading to these results has received funding from the “Programme National de Planétologie” (PNP) of CNRS/INSU, and from the European Community's Seventh Framework Programme (FP7/2007-2013) under grant agreement number RG226604 (OPTICON). AS acknowledges the support by the European Research Council/European Community under the FP7 through Starting Grant agreement number 239953. AS is supported by the European Union under a Marie Curie Intra-European Fellowship for Career Development with reference FP7-PEOPLE-2013-IEF, number 627202. ASB acknowledges funding from the European Union Seventh Framework Programme (FP7/2007-2013) under Grant agreement n. 313014 (ETAEARTH).

References

- Almenara, J. M., Deeg, H. J., Aigrain, S., et al. 2009, *A&A*, 506, 337
- Almenara, J. M., Bouchy, F., Gaulme, P., et al. 2013, *A&A*, 555, A118
- Allard, F., Homeier, D., Freytag, B. 2012, *IAU Symposium*, 282, 235
- Baranne, A., Queloz, D., Mayor, M., et al. 1996, *A&AS*, 119, 373
- Batalha, N. M., Rowe, J. F., Bryson, S. T., et al. 2013, *ApJS*, 204, 24
- Bonomo, A. S., Hébrard, G., Santerne, A., et al. 2012, *A&A*, 538, A96
- Bordé, P., Bouchy, F., Deleuil, M., et al. 2010, *A&A*, 520, A66
- Borucki, W. J., Koch, D. G., Basri, G., et al. 2011a, *ApJ*, 728, 117
- Borucki, W. J., Koch, D. G., Basri, G., et al. 2011b, *ApJ*, 736, 19
- Bouchy, F., Isambert, J., Lovis, C., et al. 2008, *EAS Publications Series*, 37, 247
- Bouchy, F., Hébrard, G., Udry, S., et al. 2009, *A&A*, 505, 853

- Bouchy, F., Bonomo, A. S., Santerne, A., et al. 2011, *A&A*, 533, A83
- Bouchy, F., Díaz, R. F., Hébrard, G., et al. 2013, *A&A*, 549, A49
- Bourrier, V., Hébrard, G., 2014, *A&A*, 569, A65
- Bressan, A., Marigo, P., Girardi, L., et al. 2012, *MNRAS*, 427, 127
- Brown, T. M., Latham, D. W., Everett, M. E., Esquerdo, G. A. 2011, *AJ*, 142, 112
- Bruntt, H., Bedding, T.R., Quirion, P.-O., et al. 2010, *MNRAS*, 405, 1907
- Burke, C. J., Bryson, S., Christiansen, J., et al. 2013, *AAS #221*, 216.02
- Butler, R. P., Wright, J. T., Marcy, G. W., et al. 2006, *ApJ*, 646, 505
- Claret, A., & Bloemen, S. 2011, *A&A*, 529, A75
- Collins, K. A., Eastman, J. D., Beatty, T. G., et al. 2014, *AJ*, 147, 39
- Colòn, K. D., Ford, E. B., Morehead, R. C. 2012, *MNRAS*, 426, 342
- Cosentino, R., Lovis, C., Pepe, F., et al. 2012, *SPIE proceedings*, 8446E
- Covino, E., Esposito, M., Barbieri, M., et al. 2013, *A&A*, 554, A28
- Cumming, A., Butler, R. P., Marcy, G. W., et al. 2008, *PASP*, 120, 531
- Deleuil, M., Almenara, J.-M., Santerne, A., et al. 2014, *A&A*, 564, A56
- Desidera, S., Sozzetti, A., Bonomo, A., et al. 2013, *A&A*, 554, A29
- Desidera, S., Bonomo, A., Claudi, R. U. et al. 2014, *A&A*, 567, L6
- Díaz, R. F., Damiani, D., Deleuil, M., et al. 2013, *A&A*, 551, L9
- Díaz, R. F., Almenara, J. M., Santerne, A., et al. 2014, *MNRAS*, 441, 983
- Dotter, A., Chaboyer, B., Jevremović, D., et al. 2008, *ApJS*, 178, 89
- Dumusque, X., Bonomo, A. S., Haywood, R. D., et al. 2014, *ApJ*, 789, 154
- Ehrenreich, D., Lagrange, A.-M., Bouchy, F., et al. 2011, *A&A*, 525, A85
- Ehrenreich, D., Désert, J.-M. 2011, *A&A*, 529, A136
- Esposito, M., Covino, E., Mancini, L., et al. 2014, *A&A*, 564, L13
- Etzel, P. B. 1981, *Photometric and Spectroscopic Binary Systems*, 111
- Faedi, F., Barros, S. C. C., Anderson, D. R., et al. 2011, *A&A*, 531, A40
- Ford, E. B. 2006, *ApJ*, 642, 505
- Fressin, F., Torres, G., Charbonneau, D., et al. 2013, *ApJ*, 766, 81
- Guillot, T., Santos, N. C., Pont, F., et al. 2006, *A&A*, 453, L21
- Guillot, T. 2010, *A&A*, 520, A27
- Guillot, T., Havel, M. 2011, *A&A*, 527,
- Guillot, T., Gautier, D. 2014, *arXiv:1405.3752*
- Hartman, J. D., Bakos, G. Á., Sato, B., et al. 2011, *ApJ*, 726, 52
- Hébrard, G., Almenara, J.-M., Santerne, A., et al. 2013a, *A&A*, 554, A114
- Hébrard, G., Collier Cameron, A., Brown, D. J. A., et al. 2013b, *A&A*, 549, A134
- Hellier, C., Anderson, D. R., Collier Cameron, A., et al. 2010, *ApJ*, 723, L60
- Howard, A. W., Bakos, G. Á., Hartman, J., et al. 2012, *ApJ*, 749, 134
- Howard, A. W., Sanchis-Ojeda, R., Marcy, G. W., et al. 2013, *Nature*, 503, 381
- Husnoo, N., Pont, F., Hébrard, G., 2011, *MNRAS*, 413, 2500
- Jenkins, J. M., Caldwell, D. A., Chandrasekaran, H., et al. 2010, *ApJ*, 713, L87
- Kipping, D. M. 2010, *MNRAS*, 408, 1758
- Kipping, D., & Bakos, G. 2011, *ApJ*, 730, 50
- Kipping, D. M. 2013, *MNRAS*, 434, L51
- Lagarde, N., Decressin, T., Charbonnel, C., et al. 2012, *A&A*, 543, A108
- Lecavelier des Étangs, A. 1997, *A&A*, 461, 1185
- Lendl, M., Anderson, D. R., Collier-Cameron, A., et al. 2012, *A&A*, 544, L72
- Lissauer, J. J., Marcy, G. W., Rowe, J. F., et al. 2012, *ApJ*, 750, 112
- Lissauer, J. J., Marcy, G. W., Bryson, S. T., et al. 2014, *ApJ*, 784, 44
- Lopez-Morales, M., Triaud, A. H. M. J., Rodler, F., et al., 2014, *ApJ*, 792, L31
- Matsumura S., Takeda G. & Rasio F. 2008, *ApJ*, 686, L29
- Matsumura, S., Peale, S. J., Rasio, F. A. 2010, *ApJ*, 725, 1995
- Mayor, M., Marmier, M., Lovis, C., et al., 2011, submitted to *A&A*, *arXiv:1109.2497*
- Moutou, C., Bruntt, H., Guillot, T., et al. 2008, *A&A*, 488, L47
- Moutou, C., Bonomo, A. S., Bruno, G., et al. 2013, *A&A*, 558, L6
- Morton, T. D., & Johnson, A. A. 2011, *ApJ*, 738, 170
- Mowlavi, N., Eggenberger, P., Meynet, G., et al. 2012, *A&A*, 541, A41
- Pepe, F., Mayor, M., Galland, F., et al. 2002, *A&A*, 388, 632
- Pepe, F., Collier Cameron, A., Latham, D. W., et al. 2013, *Nature*, 503, 377
- Perruchot, S., Kohler, D., Bouchy, F., et al. 2008, *SPIE proceedings*, 70140J
- Sanchis-Ojeda, R., Rappaport, S., Winn, J. N., et al. 2013, *ApJ*, 774, 54
- Santerne, A., Díaz, R. F., Bouchy, F., et al. 2011a, *A&A*, 528, A63
- Santerne, A., Bonomo, A., S., Hébrard, G., et al. 2011b, *A&A*, 536, A70
- Santerne, A., Díaz, R. F., Moutou, C., et al. 2012, *A&A*, 545, A76
- Santerne, A., Hébrard, G., Deleuil, M., et al. 2014, *A&A*, in press, *arXiv:1406.6172*
- Tegmark, M., Strauss, M. A., Blanton, M. R., et al. 2004, *Phys. Rev. D*, 69, 103501
- Walkowicz, L. M., Basri, G. S., 2013, *MNRAS*, 436, 1883
- Wright, J. T., Fakhouri, O., Marcy, G. W., et al. 2011, *PASP*, 123, 412

Table 6. (Electronic table available online.) Priors used for the analysis of KOI-188, KOI-195, KOI-192, and KOI-830. $\mathcal{U}(a, b)$ denotes a Uniform prior between a and b ; $\mathcal{J}(a, b)$ denotes a Jeffreys distribution between a and b ; $\mathcal{N}(\mu, \sigma^2)$ denotes a Normal distribution with a mean of μ and a width of σ^2 ; $\mathcal{N}_{\mathcal{A}}(\mu, \sigma^2, \sigma_+^2, \sigma_-^2)$ denotes an asymmetric Normal distribution with mean μ , upper width σ_+^2 , and lower width σ_-^2 ; $\mathcal{N}_U(\mu, \sigma^2, a, b)$ denotes a Normal distribution with a mean of μ , a width of σ^2 , and limited by a Uniform distribution between a and b ; $\mathcal{N}_2(\mu_1, \sigma_1^2, \mu_2, \sigma_2^2, \Delta_A)$ denotes a Bi-Normal distribution with means of μ_1 and μ_2 , widths of σ_1^2 and σ_2^2 , and Δ_A is the amplitude ratio between the two Normal distributions such that $\mathcal{N}_2(\mu_1, \sigma_1^2, \mu_2, \sigma_2^2, \Delta_A) = 0.5 \times [\mathcal{N}(\mu_1, \sigma_1^2) \times (1 - \Delta_A) + \mathcal{N}(\mu_2, \sigma_2^2) \times (1 + \Delta_A)]$; $\mathcal{S}(a, b)$ denotes a Sine distribution between a and b ; and finally $\beta(a, b)$ denotes a Beta distribution with parameters a and b (Kipping 2013).

Parameter	KOI-188	KOI-195	KOI-192	KOI-830
<i>Ephemerides and orbital parameters</i>				
Orbital period P [d]	$\mathcal{N}(3.79702, 5 \cdot 10^{-5})$	$\mathcal{N}(3.21752, 5 \cdot 10^{-5})$	$\mathcal{N}(10.29100, 5 \cdot 10^{-5})$	$\mathcal{N}(3.52563, 5 \cdot 10^{-5})$
Transit epoch T_0 [BJD _{TDB} - 2454900]	$\mathcal{N}(66.50811, 0.002)$	$\mathcal{N}(66.63102, 0.002)$	$\mathcal{N}(70.02113, 0.002)$	$\mathcal{N}(103.04727, 0.002)$
Orbital inclination i [°]	$\mathcal{S}(80, 90)$	$\mathcal{S}(80, 90)$	$\mathcal{S}(80, 90)$	$\mathcal{S}(80, 90)$
Orbital eccentricity e	0	0	$\beta(0.867, 3.03)$	0
Argument of periastron ω [°]	90	90	$\mathcal{U}(0, 360)$	90
<i>Transit parameters</i>				
Radius ratio r_p/R_*	$\mathcal{J}(0.01, 0.5)$	$\mathcal{J}(0.01, 0.5)$	$\mathcal{J}(0.01, 0.5)$	$\mathcal{J}(0.01, 0.5)$
Linear limb-darkening coefficient u_a	$\mathcal{U}(-0.5, 1.2)$	$\mathcal{U}(-0.5, 1.2)$	$\mathcal{U}(-0.5, 1.2)$	$\mathcal{U}(-0.5, 1.2)$
Quadratic limb-darkening coefficient u_b	$\mathcal{U}(-0.5, 1.2)$	$\mathcal{U}(-0.5, 1.2)$	$\mathcal{U}(-0.5, 1.2)$	$\mathcal{U}(-0.5, 1.2)$
<i>Radial velocity parameters</i>				
Systemic velocity v_0 [km s ⁻¹]	$\mathcal{U}(-50, -40)$	$\mathcal{U}(-85, -70)$	$\mathcal{U}(-30, -20)$	$\mathcal{U}(-30, -15)$
Radial-velocity semi-amplitude K [km s ⁻¹]	$\mathcal{U}(0, 1)$	$\mathcal{U}(0, 1)$	$\mathcal{U}(0, 1)$	$\mathcal{U}(0, 1)$
<i>Stellar parameters</i>				
Effective temperature T_{eff} [K]	$\mathcal{N}(5110, 100)$	$\mathcal{N}(5710, 100)$	$\mathcal{N}(5740, 90)$	$\mathcal{N}(5160, 200)$
Iron abundance [Fe/H] [dex]	$\mathcal{N}(0.35, 0.13)$	$\mathcal{N}(-0.19, 0.08)$	$\mathcal{N}(-0.19, 0.07)$	$\mathcal{N}(0.23, 0.29)$
Bulk density ρ_* [ρ_\odot]	$\mathcal{N}_{\mathcal{A}}(1.19, 0.22, 0.17)$	$\mathcal{N}(1.13, 0.26)$	$\mathcal{N}_2(0.27, 0.09, 0.66, 0.33, -0.56)$	$\mathcal{N}(1.46, 0.31)$
<i>System parameters</i>				
Distance from Earth D [pc]	$\mathcal{U}(10, 5000)$	$\mathcal{U}(10, 5000)$	$\mathcal{U}(10, 5000)$	$\mathcal{U}(10, 5000)$
Interstellar extinction $E(B - V)$ [mag]	$\mathcal{U}(0, 2)$	$\mathcal{U}(0, 2)$	$\mathcal{U}(0, 2)$	$\mathcal{U}(0, 2)$
<i>Instrumental parameters</i>				
<i>Kepler season 0 LC:</i>				
Jitter [%]	$\mathcal{U}(0, 1)$	$\mathcal{U}(0, 1)$	$\mathcal{U}(0, 1)$	$\mathcal{U}(0, 1)$
Contamination [%]	$\mathcal{N}_U(4.8, 1, 0, 100)$	$\mathcal{N}_U(3.7, 1, 0, 100)$	$\mathcal{N}_U(4.0, 1, 0, 100)$	$\mathcal{N}_U(6.6, 1, 0, 100)$
Out-of-transit flux	$\mathcal{U}(0.999, 1.001)$	$\mathcal{U}(0.999, 1.001)$	$\mathcal{U}(0.999, 1.001)$	$\mathcal{U}(0.999, 1.001)$
<i>Kepler season 0 SC:</i>				
Jitter [%]	$\mathcal{U}(0, 1)$	$\mathcal{U}(0, 1)$	$\mathcal{U}(0, 1)$	–
Contamination [%]	$\mathcal{N}_U(4.8, 1, 0, 100)$	$\mathcal{N}_U(3.7, 1, 0, 100)$	$\mathcal{N}_U(4.0, 1, 0, 100)$	–
Out-of-transit flux	$\mathcal{U}(0.999, 1.001)$	$\mathcal{U}(0.999, 1.001)$	$\mathcal{U}(0.999, 1.001)$	–
<i>Kepler season 1 LC:</i>				
Jitter [%]	$\mathcal{U}(0, 1)$	$\mathcal{U}(0, 1)$	$\mathcal{U}(0, 1)$	$\mathcal{U}(0, 1)$
Contamination [%]	$\mathcal{N}_U(3.7, 1, 0, 100)$	$\mathcal{N}_U(4.1, 1, 0, 100)$	$\mathcal{N}_U(3.2, 1, 0, 100)$	$\mathcal{N}_U(5.4, 1, 0, 100)$
Out-of-transit flux	$\mathcal{U}(0.999, 1.001)$	$\mathcal{U}(0.999, 1.001)$	$\mathcal{U}(0.999, 1.001)$	$\mathcal{U}(0.999, 1.001)$
<i>Kepler season 1 SC:</i>				
Jitter [%]	$\mathcal{U}(0, 1)$	–	$\mathcal{U}(0, 1)$	–
Contamination [%]	$\mathcal{N}_U(3.7, 1, 0, 100)$	–	$\mathcal{N}_U(3.2, 1, 0, 100)$	–
Out-of-transit flux	$\mathcal{U}(0.999, 1.001)$	–	$\mathcal{U}(0.999, 1.001)$	–
<i>Kepler season 2 LC:</i>				
Jitter [%]	$\mathcal{U}(0, 1)$	$\mathcal{U}(0, 1)$	$\mathcal{U}(0, 1)$	$\mathcal{U}(0, 1)$
Contamination [%]	$\mathcal{N}_U(5.8, 1, 0, 100)$	$\mathcal{N}_U(8.6, 1, 0, 100)$	$\mathcal{N}_U(3.1, 1, 0, 100)$	$\mathcal{N}_U(8.7, 1, 0, 100)$
Out-of-transit flux	$\mathcal{U}(0.999, 1.001)$	$\mathcal{U}(0.999, 1.001)$	$\mathcal{U}(0.999, 1.001)$	$\mathcal{U}(0.999, 1.001)$
<i>Kepler season 2 SC:</i>				
Jitter [%]	$\mathcal{U}(0, 1)$	$\mathcal{U}(0, 1)$	$\mathcal{U}(0, 1)$	–
Contamination [%]	$\mathcal{N}_U(5.8, 1, 0, 100)$	$\mathcal{N}_U(8.6, 1, 0, 100)$	$\mathcal{N}_U(3.1, 1, 0, 100)$	–
Out-of-transit flux	$\mathcal{U}(0.999, 1.001)$	$\mathcal{U}(0.999, 1.001)$	$\mathcal{U}(0.999, 1.001)$	–
<i>Kepler season 3 LC:</i>				
Jitter [%]	$\mathcal{U}(0, 1)$	$\mathcal{U}(0, 1)$	$\mathcal{U}(0, 1)$	$\mathcal{U}(0, 1)$
Contamination [%]	$\mathcal{N}_U(3.3, 1, 0, 100)$	$\mathcal{N}_U(7.1, 1, 0, 100)$	$\mathcal{N}_U(3.5, 1, 0, 100)$	$\mathcal{N}_U(8.9, 1, 0, 100)$
Out-of-transit flux	$\mathcal{U}(0.999, 1.001)$	$\mathcal{U}(0.999, 1.001)$	$\mathcal{U}(0.999, 1.001)$	$\mathcal{U}(0.999, 1.001)$
<i>Kepler season 3 SC:</i>				
Jitter [%]	$\mathcal{U}(0, 1)$	$\mathcal{U}(0, 1)$	$\mathcal{U}(0, 1)$	–
Contamination [%]	$\mathcal{N}_U(3.3, 1, 0, 100)$	$\mathcal{N}_U(7.1, 1, 0, 100)$	$\mathcal{N}_U(3.5, 1, 0, 100)$	–
Out-of-transit flux	$\mathcal{U}(0.999, 1.001)$	$\mathcal{U}(0.999, 1.001)$	$\mathcal{U}(0.999, 1.001)$	–
<i>HARPS-N 2012:</i>				
Jitter [m s ⁻¹]	$\mathcal{U}(0, 100)$	$\mathcal{U}(0, 100)$	$\mathcal{U}(0, 100)$	–
Offset [m s ⁻¹]	$\mathcal{U}(-200, 200)$	$\mathcal{U}(-200, 200)$	$\mathcal{U}(-200, 200)$	$\mathcal{U}(-200, 200)$
<i>HARPS-N 2013:</i>				
Jitter [m s ⁻¹]	$\mathcal{U}(0, 100)$	$\mathcal{U}(0, 100)$	$\mathcal{U}(0, 100)$	$\mathcal{U}(0, 100)$
Offset [m s ⁻¹]	0	0	0	0
<i>SED:</i>				
Jitter [mag]	$\mathcal{U}(0, 1)$	$\mathcal{U}(0, 1)$	$\mathcal{U}(0, 1)$	$\mathcal{U}(0, 1)$